

Anuroctoxin, a new scorpion toxin of the α -KTx 6 subfamily is highly selective for Kv1.3 over IKCa1 ion channels of human T lymphocytes.

Miklós Bagdány, Cesar V.F. Batista, Norma A. Valdez-Cruz, Sándor Somodi, Ricardo C. Rodriguez de la Vega, Alexei F. Licea, Zoltán Varga, Rezső Gáspár, Lourival D. Possani and György Panyi

Department of Biophysics and Cell Biology, University of Debrecen, Medical and Health Science Center, Debrecen 4012 Hungary (M.B., S.S., Z.V., R.G.,G.P)

²Department of Molecular Medicine and Bioprocesses, Institute of Biotechnology, National Autonomous University of Mexico, Avenida Universidad, 2001, Apartado Postal 510-3, Cuernavaca 62210 – Mexico (C.V.F.B., N.A.V-C.,R.C.R-V., L.D.P.)

³Laboratory of Molecular Immunology and Biotoxins, Centro de Investigación Científica y de Educación de Ensenada, Km 107, Carretera Tijuana-Ensenada, Ensenada BC, Mexico (A.F.L.)

Running title page

Anuroctoxin inhibits Kv1.3 channels

Corresponding author: György Panyi, M.D., Ph.D., Department of Biophysics and Cell
Biology, University of Debrecen, Medical and Health Science Center, 98. Nagyerdei
krt., Debrecen, Hungary, 4012, Phone/fax: (+36) 52 412-623, e-mail:
panyi@jaguar.dote.hu

Number of pages: 38

Number of tables: 0

Number of figures: 7

Number of references: 40

Number of words in abstract: 245

Number of words in Introduction: 734

Number of words in Discussion: 1470

List of uncommon abbreviations:

α -KTx, alpha scorpion toxin specific for K⁺-channels

MS/MS, mass spectrometer fragmentation

LC/MS, liquid chromatography/mass spectrometry

ShK: *Stichodactyla helianthus* peptide

Shaker IR: N-terminal inactivation domain deleted *Shaker* K⁺ channel

T_{EM}: effector memory T cell

T_{CM}: central memory T cell

ABSTRACT

The physiological function of T lymphocytes can be modulated selectively by peptide toxins acting on Kv1.3 K⁺ channels. As Kv1.3-specific peptide toxins are considered to have a significant therapeutic potential in the treatment of autoimmune diseases the discovery of new toxins is highly motivated. By chromatographic procedures and electrophysiological assays, using patch-clamp methodology, the isolation of a novel peptide named Anuroctoxin was accomplished, using the venom of the Mexican scorpion *Anuroctonus phaidactylus*. It has 35 amino acid residues with a molecular weight of 4082.8 atomic mass units, tightly bound by four disulfide-bridges, whose complete covalent structure was determined. It has a pyroglutamic acid at the N-terminal region and an amidated C-terminal residue. Sequence comparison and phylogenetic clustering analysis classifies Anuroctoxin into subfamily 6 of the α -KTx scorpion toxins (systematic name α -KTx 6.12). Patch-clamp experiments show that Anuroctoxin is a high affinity blocker of Kv1.3 channels of human T lymphocytes with a K_d of 0.73 nM and it does not block the Ca²⁺ activated IKCa1 K⁺ channels. These two channels play different, but important roles in T lymphocyte activation. Furthermore, the toxin practically does not inhibit *Shaker* IR, mKv1.1 and rKv2.1 channels, whereas the affinity of Anuroctoxin for hKv1.2 is almost an order of magnitude smaller than for Kv1.3. The pharmacological profile and the selectivity of this new toxin for Kv1.3 over IKCa1 may provide an important tool for the modulation of the immune system, especially in those cases when selective inhibition of Kv1.3 is required.

INTRODUCTION

Two types of ion channels dominate the K^+ conductance in human T cells: the voltage-gated Kv1.3 channel belonging to the *Shaker* family of channels (Matteson and Deutsch, 1984) and the Ca^{2+} -activated IKCa1 channel (also known as $K_{Ca3.1}$) (Grissmer et al., 1993). One major physiological function of these channels is the maintenance of a negative membrane potential, which facilitates sustained Ca^{2+} signaling during T cell activation by providing the electrical driving force for Ca^{2+} entry through voltage-independent Ca^{2+} channels. Peptide and small-molecule inhibitors of the channels depolarize the membrane resulting in the inhibition of Ca^{2+} signaling and lymphocyte proliferation (reviewed in (Panyi et al., 2004; Chandy et al., 2004)).

All quiescent human T lymphocytes express dominantly Kv1.3 channels (~300 per cell) and small number of IKCa1 channels (~8-10/cell) (Cahalan et al., 2001; Panyi et al., 2004). Depending on the nature and physiological function of the T cells, i.e. naïve, central memory (T_{CM}) and effector memory (T_{EM}) T cells (reviewed in (Sallusto et al., 2004)), their activation induces a specific change in the K^+ channel repertoire (Wulff et al., 2003). Naïve and T_{CM} cells acquire an $IKCa1^{high}Kv1.3^{low}$ channel phenotype upon activation (~500 IKCa1 and Kv1.3 channels/cell). In contrast, activation of effector memory T cells (T_{EM}) is accompanied by an increase in the number of Kv1.3 channels to ~1500/cell without any change in the IKCa1 levels, thereby the channel phenotype of the activated T_{EM} becomes $IKCa1^{low}Kv1.3^{high}$ (Wulff et al., 2003).

The difference in the K^+ channel dominance in these T cell subsets allows specific interference with their activation using selective blockers of Kv1.3 or IKCa1 channels (Chandy et al., 2004). Proliferation of encephalogenic T_{EM} cells, which play a significant role in the pathogenesis of Multiple Sclerosis, can be suppressed by selective Kv1.3 inhibitors whereas naïve and T_{CM} T cells escape Kv1.3 block-mediated inhibition

of proliferation by up-regulating IKCa1 (Wulff et al., 2003). This selective immunosuppression places the isolation of selective Kv1.3 inhibitors into the focus of ongoing research in several laboratories since these molecules are considered to have significant therapeutic potential (Chandy et al., 2004; Panyi et al., 2004)).

Scorpion venoms contain peptides that block or modulate the activity of ion channels of excitable and non-excitable cells (see review (Miller, 1995; Garcia et al., 2001; Chandy et al., 2004; Rodriguez de la Vega RC and Possani, 2004)). The K⁺-channel specific scorpion toxins (abbreviated KTx) were earlier classified into three (α , β and γ) distinct families (Tytgat et al., 1999). The α -KTx family of peptides is the best studied thus far, from which 19 subfamilies have been described (Xu et al., 2004; Rodriguez de la Vega RC and Possani, 2004). These toxins were invaluable tools in the identification of specific cellular functions mediated by ion channels and were used as molecular calipers to map the pore architecture of K⁺ channels before the three-dimensional X-ray crystallographic structure of these channels was known (Miller, 1995; Garcia et al., 2001; Jiang et al., 2003; Pardo-Lopez et al., 2002).

Several natural peptide blockers of Kv1.3 channels were isolated from scorpions having very high affinity for Kv1.3. The most potent ones, Charybdotoxin (ChTx), Margatoxin (MgTx) and Pi2 toxin from *Pandinus Imperator*, are characterized by equilibrium dissociation constants in the low nM and pM range (reviewed in (Chandy et al., 2004)). Some of these toxins, such as MgTx, display natural selectivity for Kv1.3 over IKCa1 (Leonard et al., 1992). The specificity of Kv1.3 inhibition was increased in the case of ShK toxin, a very high affinity blocker of Kv1.3 isolated from the sea anemone *Stichodactyla helianthus*, by introducing a non-natural amino acid in position 22 of the peptide (ShK-Dap²²) (Kalman et al., 1998). The diversity of the primary sequence of these peptide inhibitors and their valuable pharmacological effects

stimulate the search for new molecules in the venoms of different scorpions which were shown to be extremely rich sources of these peptides (Rodriguez de la Vega RC and Possani, 2004).

In this report we describe the isolation and functional characterization of a novel peptide toxin, named Anuroctoxin, from the venom of the scorpion *Anuroctonus phaiodactylus* belonging to the Iuridae family. This is the first report to characterize an active peptide in the venom of this scorpion. The most interesting finding, besides the unique primary structure of Anuroctoxin (systematic number α -KTx 6.12), is that it blocks Kv1.3 channels of human T lymphocytes with high affinity but does not affect calcium activated IKCa1 channels in the same cells.

MATERIALS AND METHODS

Source of venom and chemicals

Scorpions from the species *Anuroctonus phaiodactylus* were collected on the hills of Maneadero, Baja California, Mexico and electrically stimulated for venom, as earlier described (Valdez-Cruz et al., 2004). All chemicals used in this work were analytical grade reagents as indicated in our earlier publications (Valdez-Cruz et al., 2004; Batista et al., 2004). The chemicals used for the electrophysiological experiments were as earlier published (Peter et al., 2001). High quality water (bidistilled over quartz) was used for all the solutions.

Isolation procedure

The soluble venom was separated by high performance liquid chromatography (HPLC) using an analytical C18 reverse-column from Vydac (Hisperia, CA, USA) in similar conditions as described (Valdez-Cruz et al., 2004). In short, a linear gradient from solution A [0.12% (v/v) trifluoroacetic acid in water] to 60% B [0.10% (v/v)

trifluoroacetic acid in acetonitrile], run for 60 min was able to resolve many different fractions and/or components. The most active fraction as determined in our electrophysiological system (see below) was further purified using a distinct gradient from solution A to 30% solution B run for 60 min, in the same system. The purity of the peptide was ascertained by a symmetrical peak on the HPLC system, amino acid sequencing and by mass spectrometry analysis.

Amino acid sequence and mass spectrometry analysis

Automatic amino acid sequencing determination, by Edman degradation, was performed using a Beckman LF 3000 Protein Sequencer (Palo Alto, CA, USA) with the native peptide and its fragments generated by enzymatic cleavage with endopeptidases: Lysine-C (Lys-C) and Arginine-C (Arg-C), both from Boehringer (Mannheim, Germany), in the same conditions described for another component of the same venom (Valdez-Cruz et al., 2004). Mass spectrometry analysis was performed using a Finnigan LCQ^{Duo} ion trap mass spectrometer (San Jose, CA, USA) as also described in (Valdez-Cruz et al., 2004; Batista et al., 2004)).

Disulfide bridge determination

The disulfide bridge arrangement of the toxin was obtained by cleaving the native peptide with trypsin (Promega, WI, USA) and chymotrypsin (Boehringer, Mannheim, Germany) in the presence of 150 mM Tris-HCl buffer, pH 6.8, overnight at 37 °C, but without reduction and alkylation of the sample, in such way to conserve the disulfide pairing intact. Under liquid chromatography/mass spectrometer (LC/MS) separation the resulting peptides were fragmented by MS/MS in the same manner as earlier described by our group (Batista et al., 2004; Valdez-Cruz et al., 2004).

Sequence analysis and phylogenetic studies

Comparison of amino acid sequences was performed using the program ClustalX (Thompson et al., 1997) in the same conditions as earlier described by Rodríguez de la Vega RC and Possani (2004). The amino acid sequence of Anuroctoxin was also analyzed by BLAST and FASTA searches. Both retrieved only α -KTx peptides, although with low similarity scores. To perform a more in depth analysis, the full set of α -KTx currently available in the literature, plus a putative paralogous protein, a defensin-like peptide isolated from the haemolymph of the scorpion *Centruroides limpidus limpidus* (abbreviated Cll-dlp, (Rodriguez de la Vega RC and Possani, 2004), was used to generate a multiple sequence alignment (MSA) with MUSCLE (Edgar, 2004). The MSA was then slightly refined to avoid obvious structural inconsistencies. Next, the MSA was used to perform a Bayesian estimation of tree topology using MrBayes 3.0 (Ronquist and Huelsenbeck, 2003) with the Jones Taylor and Thorthon amino acid substitution model (Jones et al., 1992). Half million Markov Chain Monte Carlo (MCMC) iterations were performed allowing the program to sample between one cold and two heated chains. The phylogenetic trees were sampled every 250th generation and the resulting sets were used to calculate a consensus tree with a 50% majority rule. The convergence was achieved around the 200000th generation. For this reason the first 1000 samples (corresponding to 250000 generations) were discarded for the final consensus tree calculation. During the analysis, all the trees were rooted with Cll-dlp.

Homology modeling

The starting model was generated on Swiss-Modeller [(Schwede et al., 2003) web address: swissmodel.expasy.org] suite with the structure of HsTx1 as template (PDB code: 1quz). A user defined alignment was necessary because Anuroctoxin has one residue less than HsTx1 within the core of the molecule. This model was minimized with NAMD 2.5 (Kale et al., 1999) program until a gradient tolerance of 10^{-9} was

achieved and then a molecular dynamics simulation of 2 nanoseconds (900000 steps, 310 K) was performed to assess stability of the model. Total energy, as evaluated by NAMD, of the final model is considerably lower than the original one (ΔG 7056 arbitrary units). Minimization and molecular dynamics were performed within a square cage of 930 water molecules. Stereochemical quality of both starting and final models was assessed by WAT_CHECK [web site: www.cmbi.kun.nl/gv/whatcheck].

Cell preparation

1. Lymphocyte separation: Kv1.3 and IKCa1 currents were measured in human peripheral T lymphocytes. Heparinized human peripheral venous blood was obtained from healthy volunteers. Mononuclear cells were separated by Ficoll-Hypaque density gradient centrifugation. Collected cells were washed twice with Ca^{2+} and Mg^{2+} free Hank's solution containing 25 mM HEPES buffer (pH 7.4). Cells were cultured in a 5% CO_2 incubator at 37 °C in 24 well culture plates in RPMI-1640 supplements with 10% FCS /Hyclone, Logan, Utah, USA), 100 $\mu\text{g}/\text{ml}$ penicillin, 100 $\mu\text{g}/\text{ml}$ streptomycin and 2 mM L-glutamine at $0.5 \times 10^6/\text{ml}$ density for 3-4 days. The culture medium also contained 2.5 or 5 $\mu\text{g}/\text{ml}$ of phytohemagglutinin A (PHA-P, Sigma-Aldrich Kft, Hungary) to increase K^+ channel expression (Deutsch et al., 1986). T lymphocytes were selected for current recording by incubation with mouse anti-human CD2 (Becton-Dickinson, San Jose, CA, USA) followed by selective adhesion to Petri dishes coated with goat anti-mouse IgG antibodies (Biosource, Camarilo, CA, USA), as described by Matteson and Deutsch (Matteson and Deutsch, 1984). Dishes were washed gently five times with 1 ml of normal extracellular bath medium (see below) for the patch-clamp experiments.

2. Cytotoxic murine T cells (CTLL-2) were transiently co-transfected with plasmids for CD4 and for rat Kv2.1 (rKv2.1, kind gift from Dr. S. Korn, U. of Connecticut) or

Shaker IR channels (kind gift from Dr. G. Yellen, Harvard Medical School) at a molar ratio of 1:5 or 1:8 (32 or 48 $\mu\text{g/ml}$ total DNA) using electroporation (Deutsch and Chen, 1993). CTLL-2 cells were cultured in RPMI-1640 supplemented with 10% FBS (Hyclone, Logan, UT), 2 mM Na-pyruvate, 10 mM HEPES, 4 mM L-glutamine, 50 μM 2-mercaptoethanol, and 100 CU/ml IL-2. Before transfection, cells were cultured for 24 hours in fresh medium and collected in the logarithmic phase of growth. After harvesting, cells were suspended in Hanks'-20 mM HEPES balanced salt solution (pH 7.23) at 2×10^7 cells/ml, and the appropriate mixture of DNA was added to the cell suspension. This suspension was transferred to electroporation cuvettes (400 μl /cuvette, 4 mm electrode gap), kept on ice for 10 minutes, and then electroporated using a BTX-electroporator (San Diego, CA) with the following settings: 725 V/cm, 2350 μF , 13 Ω . The resultant time constants were 24-25 ms. Cells were incubated for an additional 10 min on ice, and transferred back to culture medium ($\sim 0.5 \times 10^6$ cells/ml) supplemented with 5 mM Na-butyrate (at 37°C, 5% CO_2). Cells were used for electrophysiology between 8-16 hours after the transfection. The selection of transfectants for electrophysiological recordings was performed using a selective monoclonal adhesion strategy, as described above, but using monoclonal mouse anti-human CD4 antibody (0.5 mg/ 10^6 cells).

3, Cos-7 cells were transiently co-transfected with plasmids for green fluorescence protein (GFP) and for hKv1.2 (pcDNA3/Hygro vector containing the full coding sequence for Kv1.2, kind gift from Dr. S. Grissmer, U. of Ulm) at a molar ratio of 1:5 using Lipofectamine 2000 reagent according to the manufacturer's protocol (Invitrogen, Carlsbad, CA, USA), and cultured under standard conditions. Currents were recorded 2-3 days after transfection. GFP positive transfectants were identified in a Nikon

TE2000U fluorescence microscope. More than 70% of the GFP positive cells expressed Kv1.2 currents.

4, L929 and B82 cells stably expressing mKv1.1 and rKv1.2 channels have been described earlier (Grissmer et al., 1994) and were kind gifts of Dr. Heike Wulff (UC Davis, CA, USA).

Electrophysiology

Whole-cell currents were measured in voltage-clamped cells using an Axopatch 200A amplifier connected to a personal computer using Axon Digidata 1200 data acquisition hardware. Series resistance compensation up to 85% was used to minimize voltage errors and achieve good voltage-clamp conditions. Pipettes were pulled from GC 150 F-15 borosilicate glass capillaries in five stages and fire polished resulting in electrodes having 2-3 M Ω resistance in the bath. The bath solution consisted of (in mM): 145 NaCl, 5 KCl, 1 MgCl₂, 2.5 CaCl₂, 5.5 glucose, 10 HEPES (pH 7.35) supplemented with 0.1 mg/ml bovine serum albumin (Sigma). The measured osmolarity of the external solution was between 302 and 308 mOsm. The internal solution consisted of (mM): 140 KF, 2 MgCl₂, 1 CaCl₂, 10 HEPES, 11 EGTA (pH 7.22) except for calcium-activated potassium current measurement, when 150 K-aspartate, 5 HEPES 10 EGTA, 8.7 CaCl₂, 2 MgCl₂, (pH 7.2) was used. In the latter case the concentration of free Ca²⁺ was 1 μ M in the pipette solution. The measured osmolarity of the internal solutions was approx. 295 mOsm. Bath perfusion around the measured cell with different test solutions was achieved using a gravity-flow perfusion setup with 8 input lines and PE10 polyethylene tube output tip with flanged aperture to reduce the turbulence of the flow. Different extracellular solutions were exchanged in the recording chamber by a gravity-driven, computer controlled system. Excess fluid was removed continuously. For data acquisition and analysis the pClamp8 software package (Axon Instruments Inc., Foster

City, CA) was used. Prior to analysis whole-cell current traces were corrected for ohmic leak and digitally filtered (3 point boxcar smoothing).

RESULTS

Isolation and structural characterization of Anuroctoxin.

The soluble venom of *Anuroctonus phaiodactylus* is separated to at least 70 different components by HPLC (see Materials and Methods), as shown in Fig.1A. The fraction eluting at 20.42 min. blocked Kv1.3 currents of human T lymphocytes with high affinity (data not shown) and was further purified as shown in the inset of Fig.1A. Some of the remaining fractions and/or components when assayed blocked the Kv1.3 currents at much higher concentration, at least two order of magnitude higher, and were considered not effective (data not shown). The inset-graphic result shows the elution of a major component (the peptide under study), plus some minor contaminants, that are discarded. This peptide applied to the amino acid sequencer gave no sequence, suggesting that it was blocked at the N-terminal region, but under mass spectrometry analysis showed the presence of a single component with a molecular weight of 4082.8 atomic mass units (a.m.u.). Three main peptides were obtained after enzymatic hydrolysis with Arg-C endopeptidase as indicated by the continuous line, under the sequence shown in Fig.1B. The most N-terminal situated one, when sequenced gave no results (it was blocked), suggesting that it was the N-terminal peptide, but when cleaved with Lys-C endopeptidase it allowed the determination of the amino acid sequence from residues in position E3 to K18, by two independent methods: automatic Edman degradation (underlined by a dotted line) and MS/MS fragmentation (underlined by dashes). The entire sequence of this peptide was also confirmed by MS/MS analysis (solid line). The subpeptide corresponding to the positions N17 to K28 was sequenced

and correctly aligned after mass fragmentation (MS/MS) of several peptides obtained by enzymatic hydrolysis as indicated under the sequence of Fig.1B. The last segment was sequenced and positioned correctly into the sequence based on the results of overlapping sequences obtained by mass fragmentation as indicated. The fact that the peptide from position C29 to K35 had an amidated lysine at the end (last amino acid), indicates the position of this subpeptide in the sequence.

Additional confirmation of the sequence came from the results aimed at the determination of the disulfide bridges, from which representative results are shown in Fig.2. For this purpose, the native toxin was digested with trypsin and chymotrypsin in a slightly acidic buffer (see Materials and Methods) without prior reduction of the sample, in such way to leave the disulfide pairing intact. This procedure, followed by LC/MS on line and tandem fragmentation (MS/MS) allowed the identification of two disulfide bridges: one between C4-C24 and the other between C10-C29 (see Fig. 2A and 2B). As it can be seen in these mass spectra the N-terminal amino acid is compatible with the presence of a pyroglutamic acid at this position, confirming that the native peptide is blocked at the most N-terminal situated residue. The third disulfide pairing formed by C14-C31 was obtained by mass fragmentation (MS/MS) of the heterodimeric peptide with molecular mass of 544.5 a.m.u. (theoretical value) and 544.5 a.m.u. found, which correspond to the sequence C14-R15 and C31-F32 of the sequence (data not shown). The amidation of K35 is clearly shown in Fig.2C. The theoretical molecular mass expected was 973.3 a.m.u., but the mass experimentally determined was 972.3 a.m.u., suggesting that the last residue was amidated. This was later confirmed by MS/MS fragmentation (Fig.2C). The completeness of the full sequence was also verified by the addition of the molecular masses found for each one of the three separated peptides after the first enzymatic cleavage with Arg-C endopeptidase. The

theoretical expected and the experimentally found molecular masses are the same (4082.8 a.m.u.). Additionally, the disulfide pairing is made between cysteines that occupy the same relative position in other α -KTx scorpion toxins. Thus, the folding of the disulfide bridges for Anuroctoxin is equivalent to the other scorpion toxins that recognize K⁺-channels.

Phylogenetic clustering analysis

When the amino acid sequence of Anuroctoxin was compared against all the known α -KTx's (81 to date), the identities fall below 50% against any of the toxins considered (Fig. 3). This low sequence relatedness is similar to the one that segregates α -KTx subfamilies 1 and 16, or between members of more divergent subfamilies (e.g. α -KTx 6). In the present case, in order to determine if Anuroctoxin belongs to one of the 19 previously assigned α -KTx subfamilies, a phylogenetic analysis was performed comprising all the peptides belonging to the α -KTx family. Initially, the sequences were aligned using MUSCLE (Edgar, 2004) and refined manually for structural inconsistencies, then a Bayesian estimation of the tree topology was performed using MrBayes 3.0 (Ronquist and Huelsenbeck, 2003). MrBayes uses Bayesian inference and Markov chain Monte Carlo sampling scheme to calculate posterior probability of a given tree topology. According to this analysis Anuroctoxin falls in a strongly supported cluster including two sisters of α -KTx subfamilies, namely 6 and 7. It is rather closely branched to subfamily 6, thus we propose the systematic number α -KTx 6.12 for Anuroctoxin. A representative Bayesian-inferred tree is shown in Fig. 4. Strongly supported clusters are highlighted by numbers under internal nodes. They represent Bayesian posterior probability ($\times 100$) of finding a given partition during the tree sampling procedure.

Block of Kv1.3 channels by Anuroctoxin

Fig.5. shows the effects of Anuroctoxin on Kv1.3 currents measured in whole-cell voltage-clamped human peripheral blood T lymphocytes. Under the experimental conditions applied (detailed in Materials and Methods and in the figure legend) the whole-cell currents were conducted exclusively by Kv1.3 channels (Peter et al., 2001). Based on 10 pS single channel conductance the number of Kv1.3 channels per T cell was between 1000 and 2000. Fig.5A displays macroscopic K^+ currents through Kv1.3 channels recorded sequentially in the same cell, before (control) and after the addition of 0.5 nM Anuroctoxin to the external solution. The displayed record in the presence of Anuroctoxin was taken after the equilibration of the block. Under these conditions approximately 50% of the channels were blocked. The block was completely reversed by perfusing the cell with toxin-free external solution (wash-out, record shown after full recovery from block).

The reversibility of the K^+ current block by 0.5 nM Anuroctoxin is also clearly demonstrated in Figs.5B and 5C. The kinetics of the channel block and its removal by wash-out is relatively fast (see Fig.5B). A more detailed analysis of the kinetics of these processes is hindered by the minimum necessary time interval between the successive data points set by the slow recovery from inactivation of Kv1.3 channels.

Fig.5C demonstrates that during the fully reversible block, 0.5 nM Anuroctoxin did not change the current-voltage relationship of the Kv1.3 channels. The threshold for activation of the current was -42.5 ± 4.8 mV (n=4) in control conditions whereas the activation threshold was -42.5 mV \pm 2.5 mV (n=4) in the presence of 0.6 nM Anuroctoxin (p>0.9). The remaining fraction of the current at each test potential was calculated as I/I_0 where I is the peak current in the presence of 0.6 nM Anuroctoxin and

I_0 is the peak current measured in control solution. Peak currents were uniformly reduced in the presence of Anuroctoxin (0.6 nM), the remaining fractions of the currents were 0.59 ± 0.07 at -20 mV, 0.51 ± 0.02 at 0 mV, 0.51 ± 0.03 at +20 mV, and 0.50 ± 0.03 at +40 mV test potentials (n=4).

Fig.5D demonstrates the dose-response curve of Kv1.3 inhibition by Anuroctoxin in the 0.05 - 10 nM concentration range. The remaining fractions of the currents (RF) were calculated at each concentration of Anuroctoxin for n=3-6 independent experiments. The dose-response curve was fit with a 3 parameter Hill equation (see legend). The resulting K_d and Hill coefficient were 0.73 nM and 0.99, respectively. The value of the Hill coefficient indicates that a single peptide interacts with the potassium channel pore, as expected from the stoichiometry of binding for several already studied K^+ channel blocking scorpion toxins (Miller, 1995).

Selectivity of K^+ channel inhibition by Anuroctoxin

Anuroctoxin was tested for specificity against IKCa1, mKv1.1, mKv1.2, hKv1.2, rKv2.1 and *Drosophila Shaker* IR channels (Fig. 6.) The potency of Anuroctoxin to inhibit IKCa1 channels was assayed for channels expressed endogenously in human peripheral blood T lymphocytes. Fig.6A shows whole-currents recorded using 1 μ M free Ca^{2+} in the pipette filling solution. This Ca^{2+} concentration is sufficient to activate maximally the Ca^{2+} activated IKCa1 potassium channels (Grissmer et al., 1993). The applied voltage-ramp evokes pure, non-voltage-gated IKCa1 currents below the activation threshold of the Kv1.3 channels, and change in the slope of the current can be used to characterize the current block (Grissmer et al., 1993). Fig. 6A demonstrates clearly that 10 nM Anuroctoxin has no blocking effect on the IKCa1 K^+ channel; the ratio of the slopes of the 10 nM Anuroctoxin treated and control curves was

1.06±0.02% (n=5, Fig. 6F). We used ChTx as a positive control in Fig. 6A, since it inhibits both IKCa1 and Kv1.3 channels. The figure shows that 10 nM ChTx significantly reduces the slope of the K⁺ current trace, the ratio of the slopes of the 10 nM ChTx-treated and control curves was 0.38±0.06 (n=5) in the membrane potential range below the activation threshold of the Kv1.3 channels. The intercept of the 10 nM ChTx-treated and control traces is between -70 mV and -80 mV (n=5) and the intercept corresponds to the 0 current level (dashed horizontal line). These data are consistent with the calculated reversal potential of a perfectly K⁺ selective conductance (-86 mV), indicating that the dominant conductance responsible for the whole-cell currents shown in Fig. 6A is K⁺-specific. The right side of Fig. 6A, in the membrane potential range above the activation threshold of Kv1.3, shows that the Kv1.3 current is almost completely inhibited in the presence of 10 nM Anuroctoxin, as expected from its sub-nanomolar affinity for Kv1.3. Current reduction in the presence of 10 nM ChTx at positive voltages, however, originates from the inhibition of both Kv1.3 and IKCa1 currents (K_d~3 nM for Kv1.3 inhibition and K_d~5 nM for IKCa1 inhibition, reviewed in (Chandy et al., 2004)).

Fig. 6 panels B-E show current traces obtained at +50 mV test potential in absence and presence of 10 nM Anuroctoxin for *Drosophila Shaker*-IR channels (lacking N-type inactivation, B), rKv2.1 channels (C), mKv1.1 channels (D) and rKv1.2 channels (E) expressed in various expression systems (see Materials and Methods). In all cases the inhibition of the whole-cell K⁺ currents by Anuroctoxin was fully reversible as indicated by the overlap of the current traces recorded before the application of the toxin and after the wash-out of the drug. The remaining fraction of the current (RF) for each channel type plus for the hKv1.2 channel at 10 nM Anuroctoxin concentration was determined for n≥4 independent experiments (Fig. 6.

panel F). The data indicates that the order of the blocking potency of Anuroctoxin for various K^+ channels is $Kv1.3 > rKv1.2 = hKv1.2 >> Shaker-IR \approx mKv1.1 \approx rKv2.1 > IKCa1$. Thus, out of the panel of channels examined, besides $Kv1.3$ channels only $Kv1.2$ channels are inhibited significantly by 10 nM Anuroctoxin. The K_d obtained from the dose-response relationship was 5 ± 0.28 nM for the $rKv1.2$ channel (data not shown). Human $Kv1.2$ channels, which differ from the rat counterpart in one amino acid in the pore region (E355 in $hKv1.2$ corresponds to D355 in $rKv1.2$), were inhibited by 10 nM Anuroctoxin essentially to the same extent as the $rKv1.2$. Assuming the interaction of a single peptide with an ion channel, the estimate of the K_d for $hKv1.2$ was calculated from the RF values obtained at a single Anuroctoxin concentration as $K_d = RF \times [toxin] / (1 - RF)$. This calculation resulted in $K_d = 6.14 \pm 0.7$ nM ($n=6$) for this channel indicating a similar potency of Anuroctoxin for the two $Kv1.2$ homologues.

Homology modeling

The subfamily α -KTx 6 contains several of the most promiscuous of all K^+ channel specific scorpion toxins, in terms of their pharmacological actions (Rodriguez de la Vega RC and Possani, 2004), though some peptides have exquisite selectivity (see for example $Pi4$, which affects $Kv1.2$ with at least 1000 fold preference over other ion-channels tested (M'Barek et al., 2003)). This is in contrast with other α -KTx subfamilies that show more homogeneous pharmacological properties. To address if some distinctive structural features would be present in Anuroctoxin that distinguish it from other α -KTx subfamily 6 members, a 3D-model was obtained by homology modeling, structural minimization and molecular dynamics (Fig. 7A). To construct the model the amino acid sequence of Anuroctoxin was aligned with those of other peptides of α -KTx subfamily 6. On the basis of this alignment the initial 3D-model was obtained in the

Swiss-Modeller suite (Schwede et al., 2003), taking the structure of HsTX1 (PDB code 1quz) as template. The model was later minimized by 3000 steps gradient on NAMD and then subjected to molecular dynamics for 2 nanoseconds, until the structure converged. The final model is considerably better than the initial one (dE > 1000 kCal) and has far fewer geometry violations as verified by the WAT_CHECK program.

DISCUSSION

In this paper we have described the isolation and the complete covalent structure determination of Anuroctoxin. This is the first peptide isolated from *Anuroctonus phaiodactylus* belonging to the Iuridae family of scorpions. When we analyzed the structure of Anuroctoxin in the context of what is known for the other KTxs (Rodriguez de la Vega RC and Possani, 2004), it is clear that its structure is quite different. Two main points have to be considered: the peptide is blocked both at the N- and C-terminal amino acids. The first residue is pyroglutamic acid (cyclic form of glutamine) similar to what was shown to be present in Charybdotoxin, and it has the last residue K35 amidated, such as it is the case of Noxiustoxin (Ntx). Thus, it is a rare example where the amino acids situated at both extremes of the peptide are blocked.

The second point is that it has a low score of similarity compared to all the other known scorpion toxins (over 120 peptides, see (Rodriguez de la Vega RC and Possani, 2004)); identities are generally lower than 40% (Fig.3). This, according to the systematic classification proposed by Tytgat et al. (1999), indicates that this peptide should be considered as the first member of a new subfamily of α -KTx scorpion toxins. However, a phylogenetic clustering analysis taking into consideration all the peptides belonging to the α -KTx family indicated that most of the trees obtained in the present sampling procedure include Anuroctoxin into the α -KTx subfamily 6, therefore α -KTx 6.12 was proposed as a systematic number for Anuroctoxin. (With few exceptions, the

phylogenetic analysis used here groups all members of the α -KTx subfamilies in a strongly supported monophyletic groups. Fourteen out of the 19 previously described subfamilies are well defined, see Supplementary figure). Overall identities of Anurotoxin with any of the peptides included in the subfamily 6 are below 45%, except for HsTx1 (α -KTx 6.3) for which it is 50%. This degree of similarity is not significantly different when comparing Anurotoxin with the peptides of subfamily 7 (43% for both Pi2 and Pi3). The results obtained here suggest that when a highly divergent family of proteins is analyzed it is recommended to use a more rigorous analytic method, rather than to conduct a simple similarity or identity search.

Patch-clamp experiments showed that Anurotoxin is potent blocker of Kv1.3 channels, the dominant voltage-gated ion channels in resting and chronically activated lymphocytes of T_{EM} phenotype (Matteson and Deutsch, 1984; Wulff et al., 2003). The block of Kv1.3 channels by Anurotoxin is very similar to the action of other scorpion toxins (Miller, 1995; Garcia et al., 2001) (Fig. 5.): the activation-gating machinery of the channels is not affected by the blocker, the current-voltage relationship in the presence of the toxin is simply scaled-down as compared to the control record. This latter argues for a voltage-independent block of the channels, which apparently contradicts the general blocking mechanism of scorpion toxins, where a positively charged central lysine (K27 in ChTx), entering the pore of the channels, confers voltage-dependence to the block (Goldstein and Miller, 1993). Since the development of, and recovery from Anurotoxin block of Kv1.3 channels is in the order of tens of seconds, the *true* voltage-dependence of block cannot be determined from the measurement of peak currents during short depolarizations to different test potentials used in this study, as discussed in details elsewhere (Peter et al., 2001). The block of Kv1.3 currents is fully reversible, the dose-response curve of Anurotoxin for Kv1.3

inhibition is characterized by a Hill coefficient ~ 1 suggesting that a single peptide interacts with the channel, similarly to other scorpion toxins.

The sequence alignment (Fig. 3) shows that K23 in Anurotoxin corresponds to K27 in ChTx, and an aromatic residue in Anurotoxin (F32) corresponds to Y36 in ChTx. Thus, the essential diad of critically positioned amino acids required for K^+ channel recognition is also found in the sequence of Anurotoxin (Dauplais et al., 1997). To determine whether the steric requirements for the formation of the essential diad are valid for Anurotoxin, its putative three-dimensional structure was generated by template modeling using the coordinates known from the structure of HsTx1 (PDB code: 1quz). This scorpion toxin was used as template, since it belongs to the same subfamily as Anurotoxin with the highest overall identity score (50%), it also has 4 disulfide bridges and displays high affinity for Kv1.3 (Lebrun et al., 1997). The model indicates that the overall structure of Anurotoxin is similar to that of ChTx, although F32 is positioned more than 7 Å apart from the α carbon of K23, a critical distance which was considered to be a hallmark for the activity of other peptide toxins (Dauplais et al., 1997).

These arguments suggest that Anurotoxin acts as a classical pore blocker of Kv1.3 channels, similarly to other scorpion toxins. Further experiments are needed to identify the unique interaction partners between Anurotoxin and the toxin receptor site in Kv1.3, which govern high affinity binding.

Regarding T cell physiology, the most important factor in the pharmacological profile of Anurotoxin is its selectivity for Kv1.3 over IKCa1, the Ca^{+} -activated K^{+} channel of human T lymphocytes. Although the limited amount of the toxin prevented the determination of a dose-response curve for the interaction with IKCa1, lack of block

at 10 nM Anurotoxin concentration allows the *lowest* estimate of ~1000 times selectivity ratio for Kv1.3 over IKCa1.

Several high affinity peptide blockers of Kv1.3 are selective for Kv1.3 over IKCa1, similarly to Anurotoxin. These include scorpion toxins, e.g. MgTx, Ntx and Kaliotoxin, and ShK toxin isolated from sea anemone. However, ion channels important in neuronal and muscle excitability are also inhibited by these toxins with nanomolar-picomolar affinities, e.g. Kv1.1 by ShK (Kalman et al., 1998) and Kaliotoxin (Grissmer et al., 1994), whereas Kv1.2 is inhibited by MgTx (Koch et al., 1997) and Ntx (Grissmer et al., 1994). Out of the panel of channels studied (Shaker, Kv1.1, Kv1.2, Kv2.1), Anurotoxin inhibited only Kv1.2 channels significantly with approximately 7-fold lower affinity than Kv1.3 channels. Within subfamily 6 of α -KTx the only high affinity blocker of Kv1.3 is HsTx1, which also inhibits Kv1.1 channels with nanomolar affinity ($K_d=7\text{nM}$) and IKCa1 channels with a modest/low affinity ($K_d=460\text{ nM}$) (Regaya et al., 2004). Thus, although phylogenetic analysis classifies Anurotoxin into subfamily 6, its pharmacological profile is similar to that of MgTx (α -KTx 2.2) and NxTx (α -KTx 2.1).

All the α -KTx peptides have very similar CS- α / β core. In particular, the members of the subfamily 6 have root mean square deviation (RMSD) values of 1.5 Angstrom for elements of the secondary structure (Fig. 7B). However, it is worth noting that the regions surrounding the common pore-blocker pharmacophore have very divergent conformations (Fig. 7B). Interestingly, three out of four positions of Pi4 proposed to be involved in Kv1.2 specificity (basic ring residues) occupy these regions. Similarly, two positions of Maurotoxin (MauTx) critical for the recognition of human Kv1.2, identified by double mutant cycle (Visan et al., 2004), occupied exactly the same positions. All peptides for which the 3D-structure is known have a basic ring

surrounding the equatorial position of the structure, apart from the site of the “functional dyad” which fits more closely to the mouth of the ion-channels (see diagram in Fig. 7C). Thus, it is tempting to speculate that the interaction of different basic residues situated in this ring of the various toxins may affect in a differential manner distinct subtypes of K⁺-channels that are recognized by these toxins, as already suggested for Pi4 (M'Barek et al., 2003), Pi1 (Mouhat et al., 2004) and MauTx (Visan et al., 2004). The two toxins from subfamily α -KTx 6 that have high affinity for Kv1.3 (Anuroctoxin and HsTx1) share a similar distribution of positively charged residues. These toxins are different from those that have high affinity for other Kv channels, v.g., MauTx and Pi4.

The selectivity of Anuroctoxin for Kv1.3 over IKCa1 confers an important pharmacological potency to this toxin for the regulation of T cell activation. This derives from the recent discovery of human T cell subtype specific expression of Kv1.3 and IKCa1 channels upon activation, and the ability of suppressing the proliferation of Kv1.3^{high}IKCa1^{low} T_{EM} cells specifically by selective Kv1.3 inhibitors. Thus, a Kv1.3-based therapy that suppresses the activation of T_{EM} cells without significant impairment of the proliferation of naïve and T_{CM} cells may establish a therapeutic potential for MS and other T cell-mediated immune diseases, such as type I diabetes mellitus, inflammatory bone resorption in experimental periodontal disease (Valverde et al., 2004) and chronic graft rejection and graft-versus-host disease sustained probably by chronically activated T_{EM} cells (Yamashita et al., 2004).

In summary, we have isolated, purified and electrophysiologically characterized a new α -KTx toxin, Anuroctoxin (α -KTx 6.12). The unique primary structure of the toxin along with its selectivity for Kv1.3 over IKCa1 makes this toxin pharmacologically interesting and valuable.

ACKNOWLEDGEMENTS

Helpful discussions with Laura Dominguez on the modeling procedures and the assistance of Saida Patricia Salas-Castillo during HPLC separation are greatly acknowledged.

REFERENCES

Batista CV, del Pozo L, Zamudio FZ, Contreras S, Becerril B, Wanke E and Possani LD (2004) Proteomics of the Venom From the Amazonian Scorpion *Tityus Cambridgei* and the Role of Prolines on Mass Spectrometry Analysis of Toxins. *J Chromatogr B Analyt Technol Biomed Life Sci* **803**:55-66.

Cahalan MD, Wulff H and Chandy KG (2001) Molecular Properties and Physiological Roles of Ion Channels in the Immune System. *J Clin Immunol* **21**:235-252.

Chandy KG, Wulff H, Beeton C, Pennington M, Gutman GA and Cahalan MD (2004) K⁺ Channels As Targets for Specific Immunomodulation. *Trends Pharmacol Sci* **25**:280-289.

Dauplais M, Lecoq A, Song J, Cotton J, Jamin N, Gilquin B, Roumestand C, Vita C, de Medeiros CL, Rowan EG, Harvey AL and Menez A (1997) On the Convergent Evolution of Animal Toxins. Conservation of a Diad of Functional Residues in Potassium Channel-Blocking Toxins With Unrelated Structures. *J Biol Chem* **272**:4302-4309.

Deutsch C and Chen L-Q (1993) Heterologous Expression of Specific K⁺ Channels in T Lymphocytes: Functional Consequences for Volume Regulation. *Proc Natl Acad Sci U S A* **90**:10036-10040.

Deutsch C, Krause D and Lee SC (1986) Voltage-Gated Potassium Conductance in Human T Lymphocytes Stimulated With Phorbol Ester. *J Physiol (Lond)* **372**:405-423.

Edgar RC (2004) MUSCLE: Multiple Sequence Alignment With High Accuracy and High Throughput. *Nucleic Acids Res* **32**:1792-1797.

- Garcia ML, Gao Y, McManus OB and Kaczorowski GJ (2001) Potassium Channels: From Scorpion Venoms to High-Resolution Structure. *Toxicon* **39**:739-748.
- Goldstein SA and Miller C (1993) Mechanism of Charybdotoxin Block of a Voltage-Gated K⁺ Channel. *Biophys J* **65**:1613-1619.
- Grissmer S, Nguyen AN, Aiyar J, Hanson DC, Mather RJ, Gutman GA, Karmilowicz MJ, Auperin DD and Chandy KG (1994) Pharmacological Characterization of Five Cloned Voltage-Gated K⁺ Channels, Types Kv1.1, 1.2, 1.3, 1.5, and 3.1, Stably Expressed in Mammalian Cell Lines. *Mol Pharmacol* **45**:1227-1234.
- Grissmer S, Nguyen AN and Cahalan MD (1993) Calcium-Activated Potassium Channels in Resting and Activated Human T Lymphocytes. Expression Levels, Calcium Dependence, Ion Selectivity, and Pharmacology. *J Gen Physiol* **102**:601-630.
- Jones DT, Taylor WR and Thornton JM (1992) The Rapid Generation of Mutation Data Matrices From Protein Sequences. *Comput Appl Biosci* **8**:275-282.
- Jiang Y, Lee A, Chen J, Ruta V, Cadene M, Chait BT and MacKinnon R (2003) X-Ray Structure of a Voltage-Dependent K⁺ Channel. *Nature* **423**:33-41.
- Kale L, Skeel R, Bhandarkar M, Brunner R, Gursoy A, Krawetz N, Phillips J, Shinozaki A, Varadarajan K and Schulten K (1999) NAMD2: Greater Scalability for Parallel Molecular Dynamics. *J Comp Phys* **151**:283-312.
- Kalman K, Pennington MW, Lanigan MD, Nguyen A, Rauer H, Mahnir V, Paschetto K, Kem WR, Grissmer S, Gutman GA, Christian EP, Cahalan MD, Norton RS and Chandy KG (1998) ShK-Dap22, a Potent Kv1.3-Specific Immunosuppressive Polypeptide. *J Biol Chem* **273**:32697-32707.

- Koch RO, Wanner SG, Koschak A, Hanner M, Schwarzer C, Kaczorowski GJ, Slaughter RS, Garcia ML and Knaus HG (1997) Complex Subunit Assembly of Neuronal Voltage-Gated K⁺ Channels. Basis for High-Affinity Toxin Interactions and Pharmacology. *J Biol Chem* **272**:27577-27581.
- Koradi R, Billeter M and Wuthrich K (1996) MOLMOL: a Program for Display and Analysis of Macromolecular Structures. *J Mol Graph* **14**:51-32.
- Lebrun B, Romi-Lebrun R, Martin-Eauclaire MF, Yasuda A, Ishiguro M, Oyama Y, Pongs O and Nakajima T (1997) A Four-Disulphide-Bridged Toxin, With High Affinity Towards Voltage-Gated K⁺ Channels, Isolated From Heterometrus Spinnifer (Scorpionidae) Venom. *Biochem J* **328** (Pt 1):321-327.
- Leonard RJ, Garcia ML, Slaughter RS and Reuben JP (1992) Selective Blockers of Voltage-Gated K⁺ Channels Depolarize Human T Lymphocytes: Mechanism of the Antiproliferative Effect of Charybdotoxin. *Proc Natl Acad Sci U S A* **89**:10094-10098.
- M'Barek S, Mosbah A, Sandoz G, Fajloun Z, Olamendi-Portugal T, Rochat H, Sampieri F, Guijarro JJ, Mansuelle P, Delepierre M, De Waard M and Sabatier JM (2003) Synthesis and Characterization of Pi4, a Scorpion Toxin From Pandinus Imperator That Acts on K⁺ Channels. *Eur J Biochem* **270**:3583-3592.
- Matteson DR and Deutsch C (1984) K Channels in T Lymphocytes: a Patch Clamp Study Using Monoclonal Antibody Adhesion. *Nature* **307**:468-471.
- Miller C (1995) The Charybdotoxin Family of K⁺-Channel-Blocking Peptides. *Neuron* **15**:5-10.

Mouhat S, Mosbah A, Visan V, Wulff H, Delepierre M, Darbon H, Grissmer S, De Waard M and Sabatier JM (2004) The 'Functional' Dyad of Scorpion Toxin Pi1 Is Not Itself a Prerequisite for Toxin Binding to the Voltage-Gated Kv1.2 Potassium Channels. *Biochem J* **377**:25-36.

Panyi G, Varga Z and Gaspar R (2004) Ion Channels and Lymphocyte Activation. *Immunol Lett* **92**:55-66.

Pardo-Lopez L, Zhang M, Liu J, Jiang M, Possani LD and Tseng GN (2002) Mapping the Binding Site of a Human Ether-a-Go-Go-Related Gene-Specific Peptide Toxin (ErgTx) to the Channel's Outer Vestibule. *J Biol Chem* **277**:16403-16411.

Peter M, Hajdu P, Varga Z, Damjanovich S, Possani LD, Panyi G and Gaspar R (2000) Blockage of Human T Lymphocyte Kv1.3 Channels by Pi1, a Novel Class of Scorpion Toxin. *Biochem Biophys Res Commun* **278**:34-37.

Peter MJ, Varga Z, Hajdu P, Gaspar RJ, Damjanovich S, Horjales E, Possani LD and Panyi G (2001) Effects of Toxins Pi2 and Pi3 on Human T Lymphocyte Kv1.3 Channels: the Role of Glu7 and Lys24. *J Membr Biol* **179**:13-25.

Regaya I, Beeton C, Ferrat G, Andreotti N, Darbon H, De Waard M and Sabatier JM (2004) Evidence for Domain-Specific Recognition of SK and Kv Channels by MTX and HsTx1 Scorpion Toxins. *J Biol Chem* **in press**.

Rodriguez de la Vega RC and Possani LD (2004) Current Views on Scorpion Toxins Specific for K⁺-Channels. *Toxicon* **43**:865-875.

Ronquist F and Huelsenbeck JP (2003) MrBayes 3: Bayesian Phylogenetic Inference Under Mixed Models. *Bioinformatics* **19**:1572-1574.

- Sallusto F, Geginat J and Lanzavecchia A (2004) Central Memory and Effector Memory T Cell Subsets: Function, Generation, and Maintenance. *Annu Rev Immunol* **22**:745-763.
- Schwede T, Kopp J, Guex N and Peitsch MC (2003) SWISS-MODEL: An Automated Protein Homology-Modeling Server. *Nucleic Acids Res* **31**:3381-3385.
- Thompson JD, Gibson TJ, Plewniak F, Jeanmougin F and Higgins DG (1997) The CLUSTAL_X Windows Interface: Flexible Strategies for Multiple Sequence Alignment Aided by Quality Analysis Tools. *Nucleic Acids Res* **25**:4876-4882.
- Tytgat J, Chandy KG, Garcia ML, Gutman GA, Martin-Eauclaire MF, van der Walt JJ and Possani LD (1999) A Unified Nomenclature for Short-Chain Peptides Isolated From Scorpion Venoms: Alpha-KTx Molecular Subfamilies. *Trends Pharmacol Sci* **20**:444-447.
- Valdez-Cruz NA, Batista CV and Possani LD (2004) Phaiodactylipin, a Glycosylated Heterodimeric Phospholipase A From the Venom of the Scorpion *Anuroctonus Phaiodactylus*. *Eur J Biochem* **271**:1453-1464.
- Valverde P, Kawai T and Taubman MA (2004) Selective Blockade of Voltage-Gated Potassium Channels Reduces Inflammatory Bone Resorption in Experimental Periodontal Disease. *J Bone Miner Res* **19**:155-164.
- Visan V, Fajloun Z, Sabatier JM and Grissmer S (2004) Mapping of Maurotoxin Binding Sites on HKv1.2, HKv1.3, and HIKCa1 Channels. *Mol Pharmacol* **66**:1103-1112.

Wulff H, Calabresi PA, Allie R, Yun S, Pennington M, Beeton C and Chandy KG
(2003) The Voltage-Gated Kv1.3 K⁺ Channel in Effector Memory T Cells As New
Target for MS. *J Clin Invest* **111**:1703-1713.

Xu CQ, Brone B, Wicher D, Bozkurt O, Lu WY, Huys I, Han YH, Tytgat J, Van
Kerkhove E and Chi CW (2004) BmBKTx1, a Novel Ca²⁺-Activated K⁺ Channel
Blocker Purified From the Asian Scorpion *Buthus Martensi* Karsch. *J Biol Chem*
279:34562-34569.

Yamashita K, Choi U, Woltz PC, Foster S, Sneller MC, Hakim FT and Fowler DH
(2004) Severe Chronic Graft-Versus-Host Disease Is Characterized by a Preponderance
of CD4⁺ Effector Memory Cells Relative to Central Memory Cells. *Blood* **103**:3986-
3988.

FOOTNOTES

Supported in part by grants: 40251Q, from the National Council of Science and Technology (Mexican Government) and IN206003 from *Dirección General de Asuntos del Personal Académico* UNAM to LDP. Support from grants OTKA TS040773, ETT 222/2003, OTKA T043087, T048740, F035251 to RG and GP, and bilateral collaboration program CONACyT-Mexico and TéT-Hungary are highly appreciated. Z.V. and G.P. were supported by Békésy Fellowship.

Reprint requests should be addressed to:

György Panyi, M.D., Ph.D.

Department of Biophysics and Cell Biology

University of Debrecen

Medical and Health Science Center

98. Nagyerdei krt.

Debrecen

Hungary

4012

Phone/fax: (+36) 52 412-623

e-mail: panyi@jaguar.dote.hu

Manuscript #: MOLPHARM / 2004 / 007187

Laboratories in the Department of Biophysics and Cell Biology, University of Debrecen and Department of Molecular Medicine and Bioprocesses, Institute of Biotechnology, Cuernavaca, contributed equally to the work.

Part of this work has been presented previously at the Annual Meeting of the Biophysical Society in Baltimore, MD, USA (Biophys J 2004;86:538A).

FIGURE LEGENDS

Fig.1. Purification and covalent structure of Anuroctoxin

(A) One milligram of soluble venom from *Anuroctonus phaiodactylus* was separated by HPLC using a C18 reverse-phase column, eluted with a linear gradient from solution A (0.12% trifluoroacetic acid in water) to 60% solution B (0.10% trifluoroacetic acid in acetonitrile) run for 60 min. The fraction labeled with asterisk was rechromatographed in the same system, run from solution A to 30% solution B in 60 min. The major component is pure Anuroctoxin and corresponds to approximately 1.1 % of the total soluble venom.

(B) The complete amino acid sequence of Anuroctoxin was obtained by a combination of direct Edman degradation and mass spectrometry fragmentation of several peptides obtained by enzymatic hydrolysis of Anuroctoxin, as indicated by the segments underlined by solid, dotted and dashed lines (see legend). The disulfide bridges are indicated by solid lines linking the cysteine residues in positions: C4-C24, C10-C29, C14-C31 and C19-C34. The N-terminal pyroglutamic acid and the C-terminal amidated lysine were determined by mass spectrometry (MS/MS) fragmentation.

Fig.2. Mass spectrometry analysis of Anuroctoxin peptides

(A) Tandem mass spectrum of the precursor ion at mass/charge (m/z) 1186.5 ($[M+2H]^{2+}$) generated by trypsin and chymotrypsin digestion after analysis by LC/MS showing the dominant fragment Y5Y2y12 with mass 1122.31, which corresponds to the loss of pyroglutamic acid at the N-terminal segment.

(B) Magnification of the collision induced dissociation spectrum shown in A, from m/z range 1160 to 2000 of the parent ion $[M+2H]^{2+}$ 1186.5, showing the bY5Y2 ion series that corresponds to the partial sequencing of the complex tri-peptide core, which in turn allowed the assignment of two disulfide pairs: C4-C24 and C10-C29.

(C) MS/MS spectrum from the precursor ion at m/z 972.32 that corresponds to the C-terminal end of Anuroctoxin. The b8 ion at m/z 955.32 corresponds to the ammonia loss from the amidated K35 residue. All y ion series values possess one a.m.u. less than the expected for the theoretical sequence inserted in the figure and all b ion series have the same experimental and theoretical values (except for b8), which defines the amidated C-terminal residue.

Fig.3. Sequence alignment of Anuroctoxin with other α -KTx member toxins.

The amino acid sequence of Anuroctoxin was compared to those of scorpion toxins from all 19 α -KTx subfamilies using the program ClustalX (Thompson et al., 1997) in the same conditions as described earlier by Rodríguez de la Vega RC and Possani (2004). One representative of each family is shown along with all members of the α -KTx subfamily 6. The I% indicates the identity score of the peptide as compared to Anuroctoxin.

Fig. 4. Phylogenetic-based clustering of Anuroctoxin.

One of the 1000 sampled trees with best probability scores in the Bayesian phylogenetic reconstruction is shown. MCMC sampling with 3 chains (2 heated) was run for 500000 iterations. The trees were sampled every 250th generations. Convergence was attained around 200000 generations and the first sampled 1000 trees were discarded. For the analysis 81 sequences of the family α -KTx were considered, plus a putative paralogous

protein (CII-dlp), used to root the tree. Groups present on the consensus tree and with a probability higher than 0.50 ($\times 100$) are mapped into this tree. For clarity only one sequence for each subfamily is shown, except for the case when a given peptide falls outside the cluster of its assigned subfamily. All the members of subfamilies 6 and 7 are shown. Branch tips are labeled with the systematic numbering of the subfamily. Within subfamily 6 the relative potency on various channels is indicated (data from: Pi1 (Peter et al., 2000; Mouhat et al., 2004), Pi4 (M'Barek et al., 2003), MauTx (Regaya et al., 2004), HsTx1 (Regaya et al., 2004)).

Fig.5. Anuroctoxin reversibly blocks whole-cell Kv1.3 currents in human T lymphocytes with high affinity.

(A) K^+ currents of a human peripheral blood T lymphocyte were recorded in whole-cell configuration during 16-ms-long test pulses to +50 mV from a holding potential of -120 mV. Test pulses were applied every 40 s. The bath was perfused continuously. Representative traces show the K^+ current before the application of the toxin (control), after the equilibration of the block in the presence of 0.5 nM Anuroctoxin (as indicated) and after the full recovery from block during the perfusion of the bath with toxin-free solution (wash-out). (B) Time courses of the development and the removal of K^+ current block. The voltage protocol and other experimental conditions were the same as in panel (A). Peak K^+ currents were determined and plotted as a function of time. Down and up arrows indicate the start and the end of perfusion with 0.5 nM Anuroctoxin, respectively. (C) Current-voltage relationship in the absence and presence of Anuroctoxin. Inset: Whole-cell K^+ currents were recorded during 200-ms-long pulses to different test potentials from a holding potential of -120 mV. Test potentials ranging from -70 to +50 mV in 10 mV increments were delivered every 40 s. The inset shows

the first 50 ms of the records belonging to the control curve measured prior to application of Anuroctoxin. Peak currents of these traces were measured and plotted as a function of the test potential (control, filled circles). The same protocol and analysis was repeated in the presence of 0.6 nM Anuroctoxin (empty circles) and after the wash-out of the toxin (down triangles). (D) Dose-response of K^+ current block by Anuroctoxin. The remaining fraction of the current (RF) was calculated as I/I_o , where I_o and I are the peak K^+ currents measured in the control solution and during bath perfusion with the test solution containing the toxin at indicated concentrations, respectively. The voltage protocol and other experimental conditions were the same as in panel (A). The superimposed solid line is the binding curve fitted to the data points: $\text{normalized current} = A \cdot K_d^n / (K_d^n + [Tx]^n)$, where $[Tx]$ indicates the toxin concentration, K_d is the dissociation constant and A is the saturating level of the expression in the absence of the toxin. The best fit resulted in $K_d = 0.73$ nM, $n=0.99$ and $A=0.96$. Error bars indicate SEM ($n=3-6$).

Fig.6. Pharmacological profile of Anuroctoxin

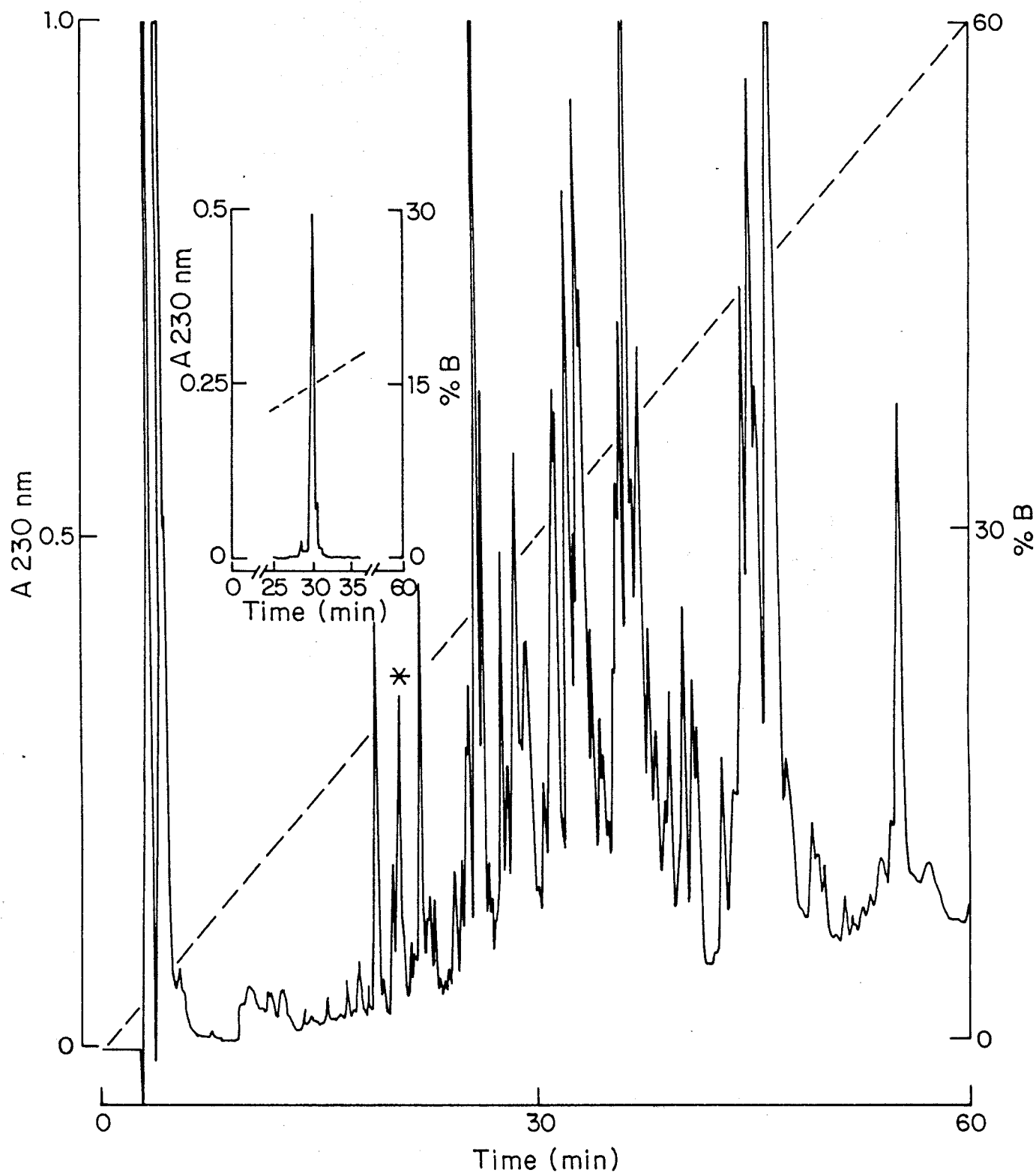
(A) IKCa1 current was measured in human peripheral lymphocytes during voltage-ramps from -120 mV to $+50$ mV with a rate of 1.176 mV/ms. Prior to the voltage ramp the holding potential was -80 mV. Both IKCa1 and Kv1.3 channels were activated in this membrane potential range. Pure IKCa1 current was measured below the activation threshold of Kv1.3 channels (left of the dashed vertical line), on the other hand a mixture of Kv1.3 and IKCa1 current was present above this voltage (right of the dashed line). Control currents were recorded in toxin-free bath solution; ChTx and Anuroctoxin were applied in the indicated concentrations. The displayed current traces in the presence of the toxins were recorded after the equilibration of the block. (B-E)

Shaker IR (B), rKv2.1 (C) mKv1.1 (D) and rKv1.2 (E) currents were evoked by voltage-clamp protocols shown in the insets of the panels before (control), during the external application of 10 nM Anuroctoxin and after its removal by wash-out. In all cases sufficient time was allowed between recordings at the holding potential for the complete recovery of the channels from inactivation (interpulse intervals were 5 s, 30 s, 15s and 15s for *Shaker* IR, Kv2.1, Kv1.1 and Kv1.2 records, respectively). (F) Remaining fraction of the currents (RF) was calculated as I/I_o , where I_o and I are the peak K^+ currents measured in the control solution and during bath perfusion with the test solution containing 10 nM Anuroctoxin, respectively. Data are represented as mean \pm SEM for $n \geq 4$ independent determinations. Ion channels were expressed endogenously in human T cells (Kv1.3, IKCa1) or in various expression systems (CTLL-2 for *Shaker*-IR and rKv2.1, L929 for mKv1.1, B82 for rKv1.2 and Cos-7 for hKv1.2, see Materials and Methods for details). Pulse protocols were the same as in Fig 5A and panels A-E of this figure.

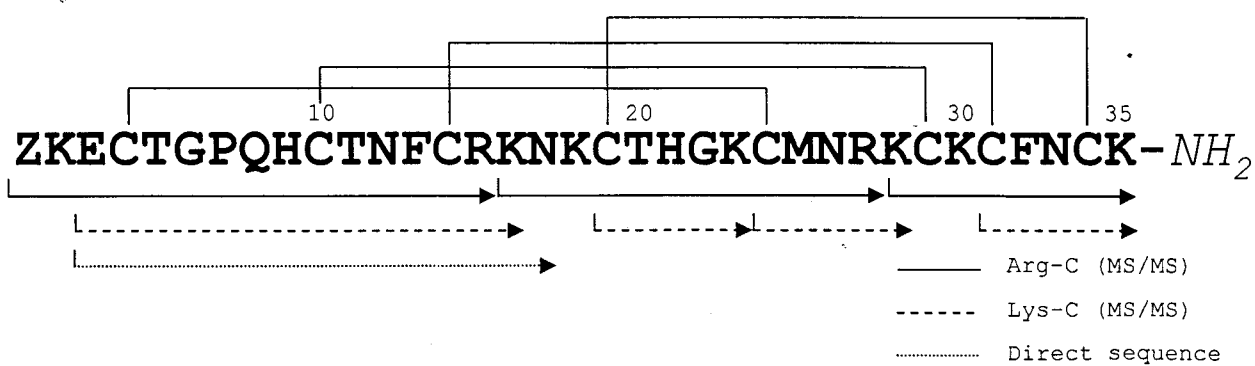
Fig. 7. Homology model of Anuroctoxin and comparison with other scorpion toxins. The model of Anuroctoxin (orange) calculated in Swiss-Model suite and refined with NAMD, and representative solution structures of Maurotoxin (1txm, purple), HsTx1 (1quz, dark green), Pi4 (1n8m, pale green) and IsTx (1wmt, grey) are displayed with MolMol (Koradi et al., 1996). A) Ribbon diagram of the final model, showing the 4 disulfide bridges. B) Superimposition of the structures of the α -KTx subfamily members (RMSD 1.39 Å for MauTx, 1.39 Å for HsTx1, 1.38 Å for Pi4 and 1.38 Å for IsTx). Arrows indicate zones of high structural variability. C) “Basic ring” (space filled representation) and “functional dyad” (ball and chain representation) residues of HsTx1, Pi4, Maurotoxin (MauTx) and Anuroctoxin in the same orientation. Note the differences

in spatial localization of the basic ring residues. The putative contact amino acids on the respective channels (Pi4 with rKv1.2 (M'Barek et al., 2003) and MauTx with human Kv1.2 (Visan et al., 2004)) are indicated.

A



B



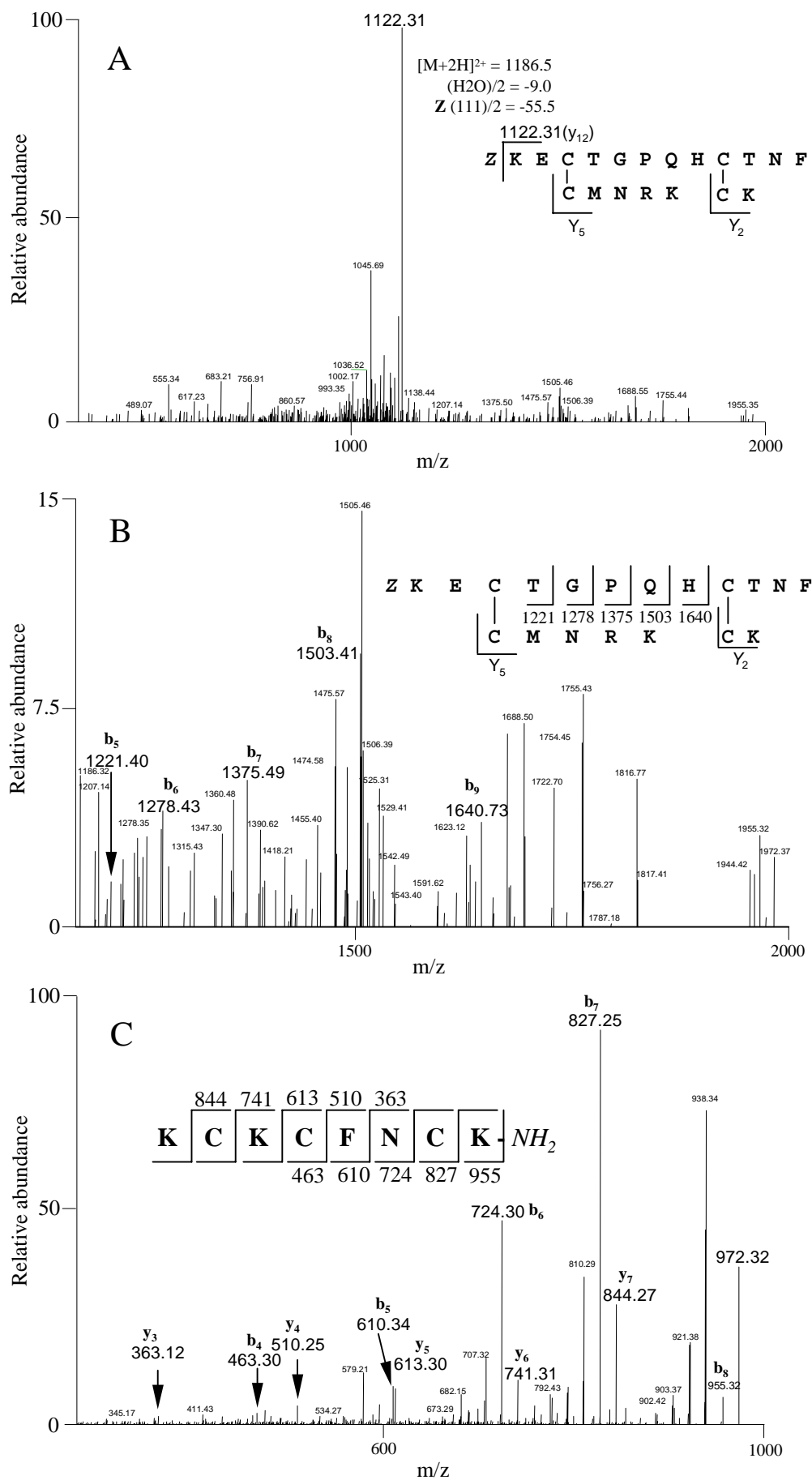


Fig. 2.

		10	20	30	40	%I
					
1.1	ChTx (2crd)	---	ZFTNVSC	TTSKECWSVCQRLHNTSRG- K CMN---	KKCRCYS----	31
2.1	Ntx (1sxm)	---	TIINVKCTSPKQCSKPKCELYGSSAGAK K CMN---	GKCKCYNN---		37
3.1	Ktx (2ktx)	--	GVEINVKCSGSPQCLKPKCKDA-GMRFG- K CMN---	RKCHCTP----		32
4.1	TsTXKa (1hp2)	---	VFINAKCRGSPECLPKCKEAIGKAAG- K CMN---	GKCKCYP----		33
4.2	Tsk (1tsk)	---	VVIGQRCYRSPDCYSACKKLVGKATG- K CTN---	GRCDC-----		26
5.1	ScytX (1scy)	-----	AFCN-LRMCQLSCRS-LGLL-G- K CIG---	DKCECVKH---		28
6.1	Pi1	-----	LVKCRGTSDCGRPCQQQTGCPNS- K CIN---	RMCKCYG-C--		36
6.2	MauTx (1txm)	-----	VSGTSGKDCYAPCRKQTGCPNA- K CIN---	KSCKCYG-C--		42
6.3	HsTx1 (1quz)	-----	ASCRTPKDCADPCRKETGCPYG- K CMN---	RKCKCNR-C--		50
6.4	Pi4 (1n8m)	----	IEAIRCGGSRDCYRPCQKRTGCPNA- K CIN---	KTCKCYG-CS-		34
6.5	Pi7 (1qky)	----	DEAIRCTGTDKCYIPCRYITGCFNS- R CIN---	KSCKCYG-CT-		34
6.6	OcKTx1	----	AEVIKCRTPKDCAGPCRKQTGCPHG- K CMN---	RTCRCNR-C--		45
6.7	OcKTx2	----	AEVIKCRTPKDCADPCRKQTGCPHG- K CMN---	RTCRCNR-C--		45
6.8	OcKTx3	----	AEVIKCRTPKDCAGPCRKQTGCPHA- K CMN---	KTCCRHR-C--		39
6.9	OcKTx4	----	AIIRCSGTRECYAPCQKLTGCLNA- K CMN---	KACKCYG-CV-		39
6.10	OcKTx5	----	AEVIRCSGSKQCYGPKQQTGCTNS- K CMN-----	CKCYG-C--		37
6.11	IsTx (1wmt)	---	VHTNI PCRGTSDCYEPCEKKTNCARA- K CMN---	RHCNCYNNCPW		34
6.12	Anuroctoxin	-----	ZKECTGPQHCTNFRCRKNK-CTHG- K CMN---	RKCKCFNCK--		100
7.1	Pi2 (2pta)	-----	TISCTNPKQCYPHCKKETGYRNA- K CMN---	RKCKCFGR---		44
8.1	P01 (1acw)	-----	VSC---EDCPEHCSTQKAQA--- K CDN---	DKCVCEPI---		25
9.1	Bmp02 (1du9)	-----	VGC---EECPMHCKGKNAKP---TCDD---	GVCNCN-V---		17
10.1	CotX (1pju)	-----	AVCV-YRTCDKDKCR-RGYRSG- K CIN---	NACKCYPY---		25
11.1	PBTx1	--	DEEPKESCS-DEMCVIYCKG-EEYSTG-VCDG--	PQCKCSD----		22
12.1	Btx (1c55)	WCSTCLDLACGASRECYDPCFKAFGRAHG- K CMN---	NKCRCYT----			31
13.1	Tc1 (1jlz)	-----	AC---GSCRKKCK-----GSG- K CIN---	GRCKCY-----		28
14.1	BmKK1	---	TPFAIKCATDADCSRKCP---GNP---SCRN---	GFCACT-----		18
15.1	Aa1	--	QNETNKKCQ-GGSCASVCRRVIGVAAG- K CIN---	GRCVCYP----		30
16.1	Tamulotx	---	DLIDVKCISSQECWIACKKVTGRFEG- K CQN---	RQCRCY-----		26
17.1	BmKK4 (1klh)	-----	QTQCQSVRDCQQYCLT----PDR--CSY---	GTCYCKTT---		20
18.1	Tc32	---	TGPQTTCQ-AAMCEAGCKG-LGKSME-SCQG---	DTCKCKA----		21
19.1	BmBKTx (1q2k)	-----	AACY-SSDCRVKCVA-MGFSSG- K CIN---	SKCKCYK----		31
C11-dlp		-----	AC-QFWSCNSSCISR-GYRQG-YCWGIQYKYCQCQ-----			18

Fig.3.

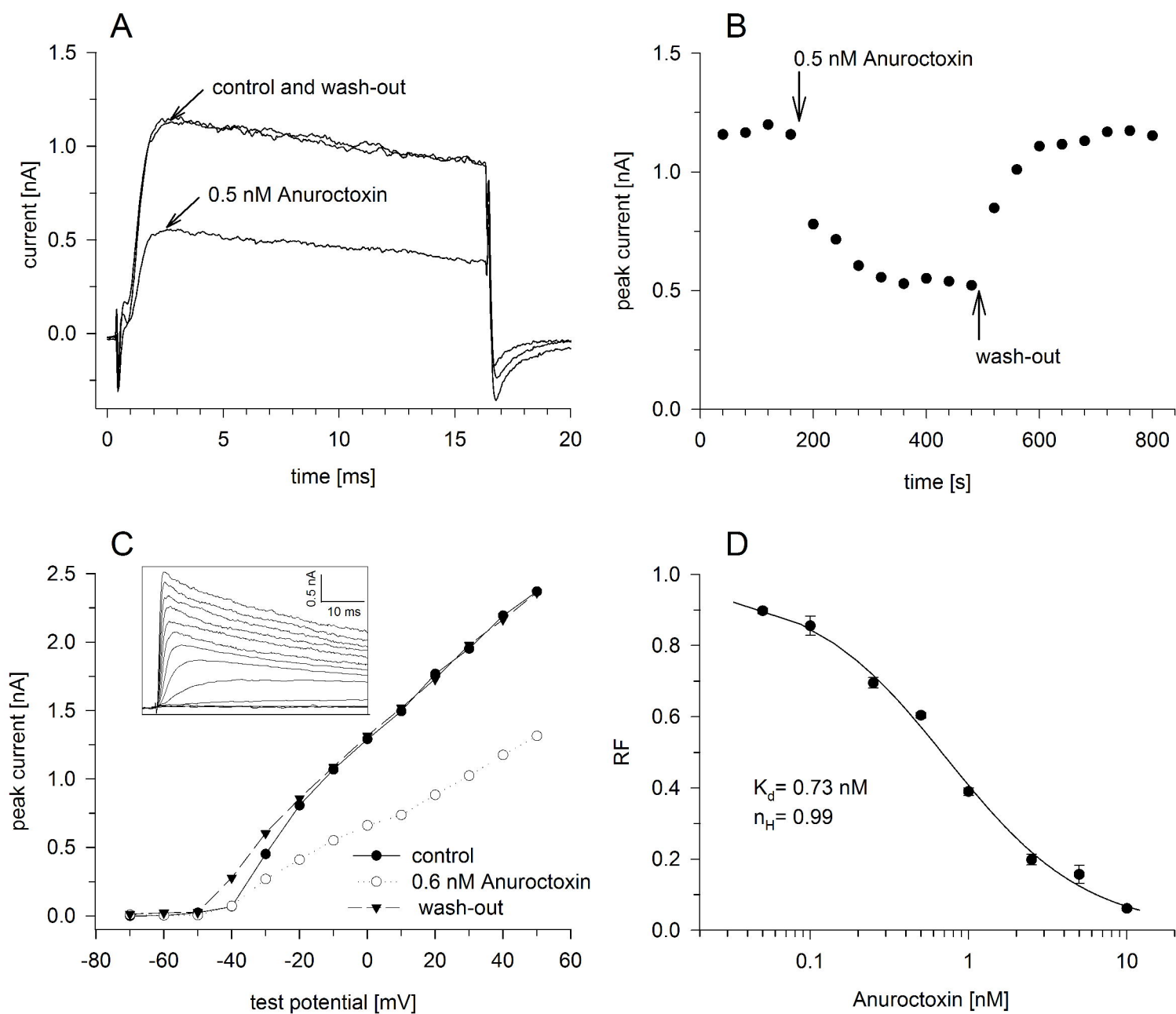


Fig. 5.

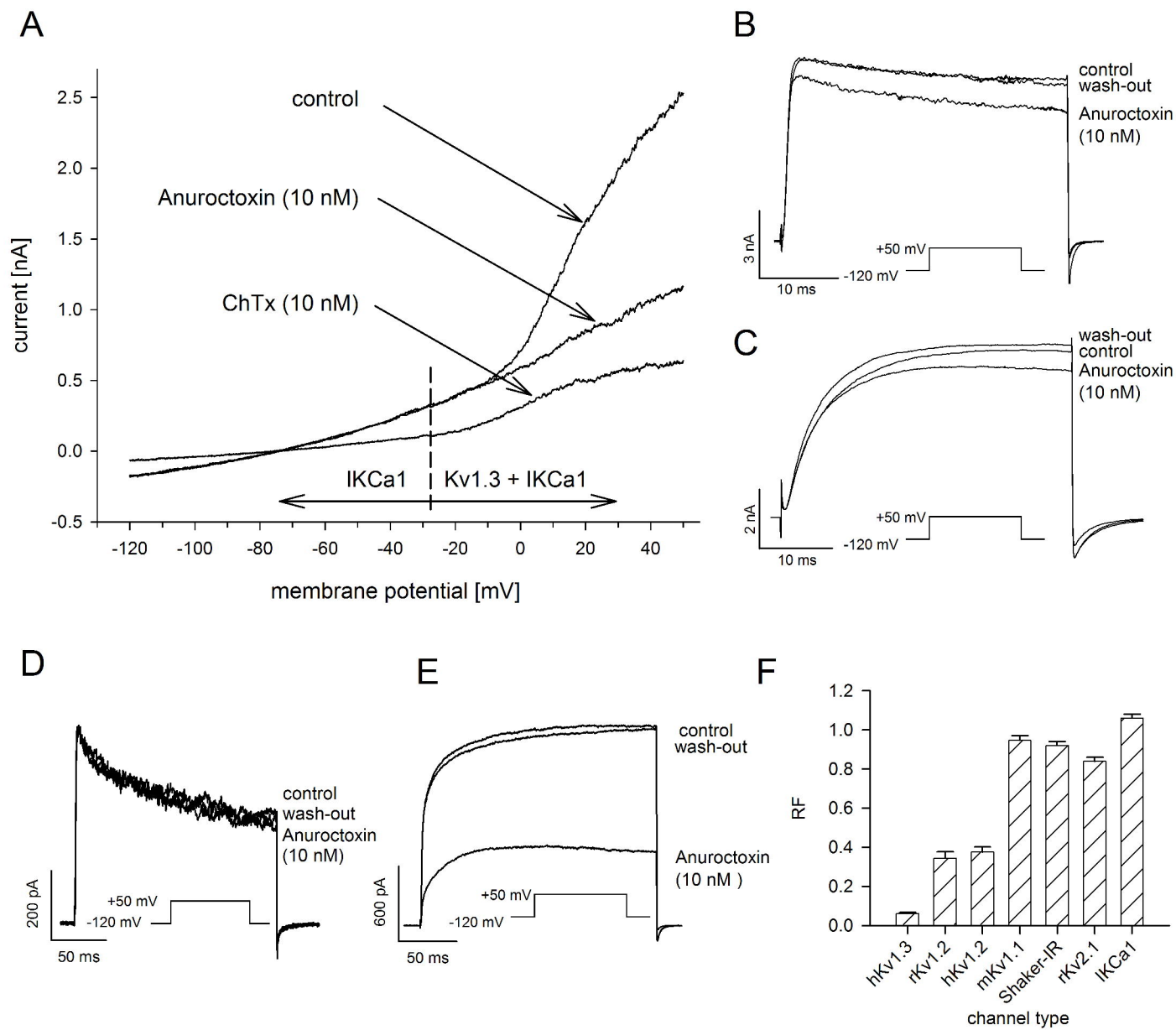
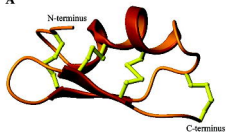


Fig. 6.

A**B****C**